Photoelectrochemistry of a Substituted-Ru(bpy)$_3^{2+}$-Labeled Polyimide and Nanocrystalline SnO_2 Composite Formulated as a Thin-Film Electrode

Weijin Li, Hiroyuki Osora, Luis Otero, Dean C. Duncan, and Marye Anne Fox*

Department of Chemistry and Biochemistry, The University of Texas at Austin, Austin, Texas 78712

Received: August 25, 1997; In Final Form: November 3, 1997

Composite nanocrystalline SnO_2 thin films layered with a polyimide sensitizer to which is attached a Ru(bpy)$_3^{2+}$ derivative were prepared by spin-coating. Photophysical and electrochemical properties of such composite films, when formulated as polymer-modified electrodes, are described. Excitation spectra of both composite films and of the dissolved polymer indicate substantial ground-state aggregation of the pendent ruthenium(II) complexes. Because of high loading of the pendent ruthenium(II) complex in the composite, high adsorptivity by the dye is attained. A maximum incident photon-to-photocurrent conversion efficiency (IPCE%) of 16% was observed upon monochromatic photosensitization at 460 nm.

Introduction

The photoelectrochemical response of a metal oxide nanoparticulate (Q-particles)[1−5] thin film sensitized by an attached dye is an excellent probe for interfacial electron transfer.[3] Increased interest in such measurements follows from the use of such electrodes as key components in arrays for photochemical water-splitting,[3,4] heterogeneous photocatalysis,[5] and photocatalytic water purification.[6] Significantly enhanced charge separation has been observed in a system employing such a semiconductor nanoparticle electrode as a relay for transporting electrons from an adsorbed excited donor to a conductive dark contact.[2,7]

A significant number of nanocrystalline thin-film electrodes have employed low molecular weight inorganic[2,3,8−13] and organic dyes[14−18] as photosensitizers when adsorbed on the semiconductor metal oxide. However, little detail is known about the efficiency of photoinduced electron transfer on such nanoparticulate semiconductor films when the photosensitization is accomplished with a polymeric dye.[18] In this study, the synthesis and characterization of a rigid polyimide **3** labeled with pendent Ru(bpy)$_3^{2+}$ derivative are described (Scheme 1). Composite thin-film electrodes are then fashioned by layering this polymeric dye on thin films of n-type nanocrystalline SnO_2, as either single- or multiple-layered structures. These polymer composite electrodes are then investigated by absorption and fluorescence spectroscopy and by photoelectrochemical measurements to define their utility as light responsive wide-bandgap semiconductors.

SCHEME 1: Synthesis of a Substituted Ru(bpy)$_3^{2+}$-Labeled Polyimide (3)

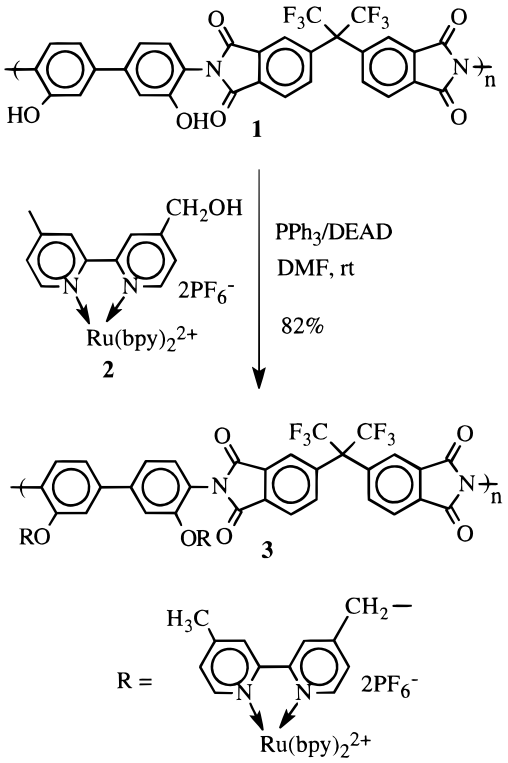

Experimental Section

General Methods. Melting points were measured by a Melt-temp apparatus (uncorrected). Nuclear magnetic resonance (NMR) spectra were recorded on Bruker AC-250 (250 MHz) spectrometer. Chemical shifts are reported as δ values relative to an internal deuterated solvent or tetramethylsilane (TMS). Absorption spectra were recorded on a Shimadzu UV-3101 scanning spectrophotometer.

Glass transition (T_g) and thermal decomposition temperatures were recorded on a Perkin-Elmer differential scanning calorimeter (DSC7) and thermogravimetric analyzer (TGA7), respectively. The scanning speeds for the DSC and TGA were 40 and 30 °C/min, respectively. Film thicknesses were measured by profilometry (Alpha-step Model 100, Tencor Instruments).

Cyclic voltammetry was performed on a Princeton Applied Research (PAR) Model 173 potentiostat. Glassy carbon electrodes were employed as working electrodes in deoxygenated acetonitrile (MeCN) containing 0.1 M tetrabutylammonium perchlorate (TBAP) as the supporting electrolyte, with a saturated calomel electrode (SCE) as reference and a Pt wire as the counter electrode.

Solution fluorescence spectra were recorded on an SLM Aminco SPF-500C fluorometer. Surface fluorescence spectra

S1089-5639(97)02757-6 CCC: $15.00
Published on Web 01/13/1998

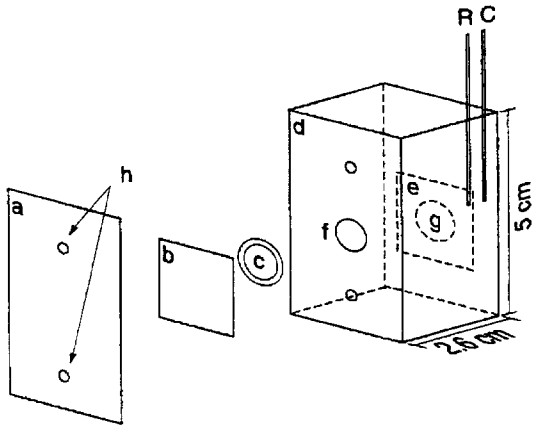

Figure 1. Schematic diagram of the cell used for the photoelectrochemical measurements: (a) Plexiglas sheet, (b) working electrode, (c) O-ring (1.2 cm diameter), (d) Teflon cell, (e) quartz glass plate, (f) hole exposing the working electrode to the solution, (g) hole (1.0 cm diameter) exposing the quartz plate to the solution, (h) screw holes. C and R are the counter electrode and reference electrode, respectively.[19]

were collected under identical conditions on a SPEX Fluorolog 2 instrument in the front-face mode. The instrument contains a 450 W Xe lamp, a Hamamatsu R508 photomultiplier, and double-grating monochromators on both the excitation and emission sample compartments of a SPEX DM3000 controller unit interfaced with the Fluorolog instrument. Samples were held in a custom-designed holder that places the electrode at a fixed distance from both the excitation source and the detector, allowing reproducible fluorescence intensities to be recorded.

Photoelectrochemical Measurements. Photoelectrochemical experiments of polymer-modified electrodes were carried out in a electrochemical cell[19] equipped with a optically flat quartz window, a Ag/AgCl reference electrode, and a Pt foil auxiliary electrode (Figure 1). The measurements were conducted in aqueous hydroquinone (H_2Q, 0.01 M) containing NaH_2PO_4 as electrolyte (0.05 M) at pH 5.2 that had been thoroughly deoxygenated by bubbling with N_2. A PAR Model 173 potentiostat, a Model 179 digital coulometer, and a Model 175 universal programmer were used in all photoelectrochemical measurements, and the results were recorded on a Houston Instruments Model 2000 $x-y$ recorder.

Photocurrent action spectra for the polymer-modified electrodes were obtained with a 150 W high-pressure Xe lamp as the excitation light source, with the collimated light beam passing through an Oriel 77250 grating monochromator to select the excitation wavelength as the steady-state photocurrent was recorded. The electrodes were located at the focus of condensing lens (illuminated area = 0.78 cm^2) held 25 cm from the monochromator. The incident light intensities at the different wavelengths were measured with an IL700 International Light Research Radiometer.

Materials. Optically transparent electrodes (1.5 × 1.5 cm^2) were cut from indium tin oxide (ITO) coated glass plates (1.3 mm thickness of ITO, 100 Ω/square) obtained from Delta Technologies. An aqueous colloidal suspension of SnO_2 (15%) with an average particle diameter of 20−30 Å (Alfa Chemicals) was used as received. Hydroquinone (Aldrich) was recrystallized from toluene. Monobasic sodium phosphate (Fisher) was used as received.

Diethyl azodicarboxylate (DEAD), triphenylphosphine (PPh_3), bipyridine (bpy), 4,4′-dimethyl-2,2′-bipyridine, *m*-chloroperbenzoic acid, and ammonium hexafluorophosphate (NH_4PF_6, Aldrich), and ruthenium trichloride hydrate ($RuCl_3 \cdot 3H_2O$, Lancaster) were used as received. Anhydrous tetrahydrofuran (THF) was freshly distilled from Na/benzophenone under N_2. High-purity CH_3CN (Burdick & Jackson) was used for all spectroscopy and electrochemical measurements. TBAP (Aldrich) was recrystallized from absolute ethanol before use.

TABLE 1: Structures of Electrodes I−VIII

electrodes	structure
I	SnO_2 (12 × application)
II	**I** + 1 layer of **1** (10 mg/mL in THF)
III	**I** + 1 layer of **3** (10 mg/mL in MeCN)
IV	**I** + 1 layer of **3** (40 mg/mL in MeCN)
V	3 × (1 × application of SnO_2 + 1 layer of **3** (10 mgL))
VI	4 × (1 × application of SnO_2 + 1 layer of **3** (10 mgL))
VII	**I** + solution impregnation by **2** (2×10^{-4} M) in ethanol
VIII	ITO + 1 layer of **3** (10 mg/mL in MeCN)

Polyimide **1** was prepared using a procedure described by Ho et al.[20] [4-(Hydroxymethyl)-4′-methyl-2,2′-bipyridine]bis-(2,2′-bipyridine)ruthenium(II) hexafluorophosphate, $\{Ru^{2+}(4\text{-}CH_2OH\text{-}4'\text{-}Mebpy)(bpy)_2\}$ $(PF_6^-)_2$ (**2**),[21−23] was attached to **1** by a Mitsunobu reaction[24] via an ether linkage (Scheme 1).

Synthesis of Substituted $Ru(bpy)_3^{2+}$-Labeled Polyimide (3). Polyimide **1** (0.3 g, 0.5 mmol of repeat unit), PPh_3 (0.8 g, 3 mmol), and the ruthenium tris(bipyridyl) derivative **2** (1 g, 1 mmol) were dissolved successively in dry DMF (30 mL). The flask was flushed with dry nitrogen. Diethyl azodicarboxylate (DEAD, 0.5 g, 3 mmol) was added dropwise to the solution. A red precipitate, which formed immediately, dissolved into the solution after stirring at room temperature for 1 h. The reaction mixture was further stirred at room temperature for 48 h under N_2 and was then added dropwise to 500 mL of methanol containing 3 equiv of NH_4PF_6. The collected precipitate was redissolved in MeCN (30 mL) and was reprecipitated into methanol−NH_4PF_6 (500 mL). The polymer was further purified by precipitating into ether (500 mL) twice from MeCN (30 mL). The red precipitate was dried at 80 °C under vacuum overnight to provide 1 g (82%) of product with ∼100% $Ru(bpy)_3^{2+}$ loading: ^{1}H NMR (CD_3CN) δ 2.52 (br, s, 6 H), 6.05 (br, s, 4 H), 7.86−9.01 (br, 56 H); UV/vis (MeCN) λ_{max} ($\epsilon \times 10^{-4}$ M^{-1} cm^{-1}) 454 (1.4) nm; fluorescence (MeCN) λ_{max} 615 nm; DSC T_g > 400 °C; TGA 5% weight loss beginning at 480 °C.

Preparation of Polymer-Modified Nanocrystalline SnO_2 Semiconductor Thin-Film Electrodes (I−VIII). A structural summary of the composite electrodes is provided in Table 1. Kamat's procedure[9,13,25] was modified slightly to prepare SnO_2 or composite SnO_2−polymer thin-film electrodes. Spin-coating was used to apply sequentially both the colloidal semiconductor and the dye-loaded polymer layers. A small aliquot (0.1 mL) of a dilute SnO_2 colloidal suspension (1.5 wt %) containing a surfactant (0.01 wt % Triton X-100, Aldrich) was applied onto a clean ITO surface using a Model P6204-A Specialty Coating System at a speed of 3500 rpm for 35 s. The electrode was then dried at 200 °C for 5 min. A thick film of pristine SnO_2 was obtained by repeating the application 12 times. The final film was annealed at 400 °C for 1 h, affording a film **I** with a thickness of 0.18 μm as measured by profilometry.

A solution of polymer **3** or **1** was spin-coated onto the electrode **I**. The double layer composite films produced from polymer **1** in THF at a concentration of 10 mg/mL and from polymer **3** in MeCN at concentrations of 10 and 40 mg/mL, respectively, are called electrodes **II**, **III**, and **IV**, respectively (Table 1 and Figure 2).

In addition, multilayer laminated electrodes were constructed. A layer of SnO_2 was first spin-coated onto ITO as described above, followed by a layer of **3** (10 mg/mL in MeCN). This

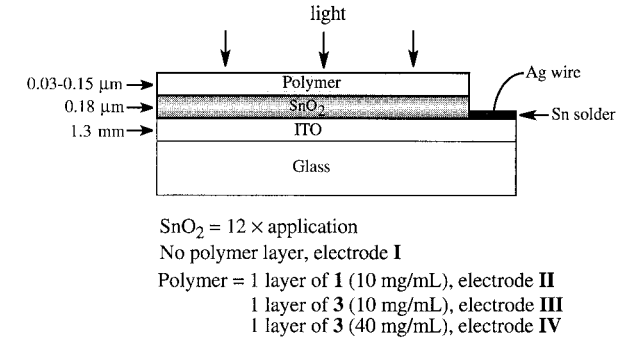

Figure 2. Schematic diagram of electrodes **I**−**IV**.

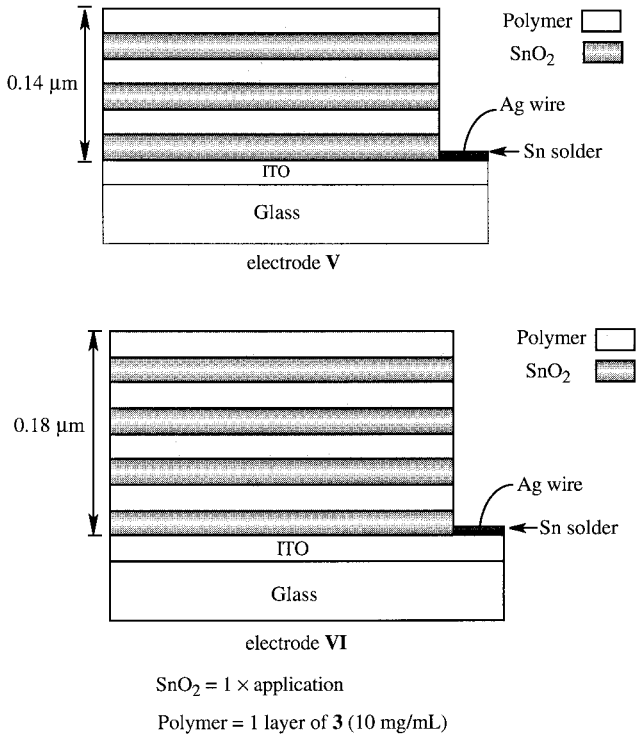

Figure 3. Schematic diagram of the laminated electrodes **V** and **VI**.

two-layer sequence was applied three and four times, respectively, to obtain electrodes **V** and **VI** (Table 1 and Figure 3). The thicknesses of the deposited SnO_2−polymer layers on electrodes **V** and **VI**, as indicated by profilometry, are 0.14 and 0.18 μm, respectively. Between each application, the electrodes were heated at 200 °C for 5 min.

To compare the spectral properties of polyimide **3**-derivatized electrodes (**III**−**VI**) with that of a thin-film SnO_2 electrode to which was adsorbed complex **2**, electrode **I** was soaked in a warm solution of **2** in ethanol (2×10^{-4} M) for 3 h. The resulting electrode (**VII**, Table 1) was then dried under a slow stream of Ar. Electrode **VII** is only suitable for solid-state spectroscopy studies because **2** is soluble in the electrolyte used for the photoelectrochemical measurements with electrodes **I**−**VI**. An additional control electrode **VIII** was prepared by spin-coating **3** (10 mg/mL in MeCN) directly onto ITO.

Results and Discussions

Synthesis and Characterization of Polyimide 3. Because the Mitsunobu reaction is sensitive to water,[24] the hydroxy-derivatized ruthenium(II) complex **2** was attached to polyimide **1** in anhydrous DMF containing an excess of DEAD and PPh_3. Integration of the relevant peaks in the ^{1}H NMR spectrum was

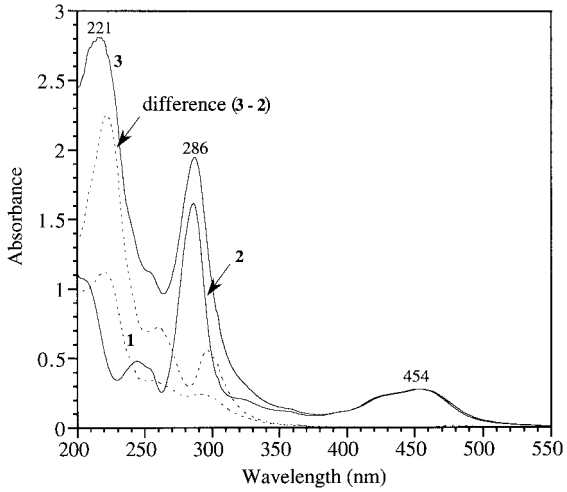

Figure 4. Absorption spectra of **1** (1×10^{-5} M), **2** (2×10^{-5} M), and **3** (2×10^{-5} M) in degassed MeCN at room temperature. The difference spectrum between **2** and **3** is also shown.

employed to evaluate the loading of **2**. The ^{1}H NMR resonance at 10.5 ppm assigned to hydroxyl protons in **1**[20] is completely depleted in the ^{1}H NMR spectrum of polyimide **3**, indicating essentially complete loading of the ruthenium complex to each pendent hydroxyl group. Polyimide **3** is highly thermally stable, with a glass transition temperature (T_g) >400 °C and a thermal decomposition temperature >480 °C, respectively.

Complex **2** has absorption maxima at 286 nm ($\epsilon = 8.0 \times 10^4$ M^{-1} cm^{-1}) and 454 nm ($\epsilon = 1.4 \times 10^4$ M^{-1} cm^{-1}), whereas polymer **1** shows absorption bands only in the ultraviolet region, with maxima at 221 nm ($\epsilon = 2.2 \times 10^5$ M^{-1} cm^{-1}), 260 nm ($\epsilon = 7.2 \times 10^4$ M^{-1} cm^{-1}) and 294 nm ($\epsilon = 5.5 \times 10^4$ M^{-1} cm^{-1}, Figure 4). The absorption maxima observed for **3** are consistent with the incorporation of **2** onto **1**. Furthermore, the difference absorption spectrum between **2** and **3** exhibits the same absorption characteristics as does polymer **1**. The metal-to-ligand charge-transfer absorption band at 454 nm of **3** is identical with that of the monomer **2**, indicating that chromophore **2** retains its intrinsic electronic properties upon attachment to polyimide **1**.

Characteristics of Porous SnO_2 Electrodes. A transparent thin-film electrode **I** fashioned from sequentially deposited layers of nanocrystalline SnO_2 exhibits photoelectrochemical characteristics similar to those described by Kamat.[13] The magnitude of the photocurrent produced by photosensitization by zinc porphyrin adsorbed onto an analogous nanocrystalline SnO_2 thin film has been shown to increase linearly with film thickness for very thin films but to level off at thicknesses >0.25 μm.[26] This observation indicates that nanocrystalline SnO_2 thin films such as **I** are highly porous and that the net efficiency of electron hopping among the constituent SnO_2 nanoparticles before reaching the ITO conductive support reaches a maximum at a SnO_2 thickness of about 0.25 μm. Although more photons are harvested by a thicker dye-coated SnO_2 film (because of higher loading of the sensitizer), there is a higher probability of recombination of the photogenerated electrons and holes when these carriers must partake of a large number of random hops as they migrate through the thicker film because of the larger number of colloidal particles and grain boundaries encountered.[9]

Electrode **I** (precoated with 12 deposited layers of nanoparticle SnO_2) has a thickness of 0.18 μm. It is highly transparent in the visible region (>400 nm) with an absorption onset at around 350 nm, corresponding to a bulk bandgap of 3.5 eV.[25]

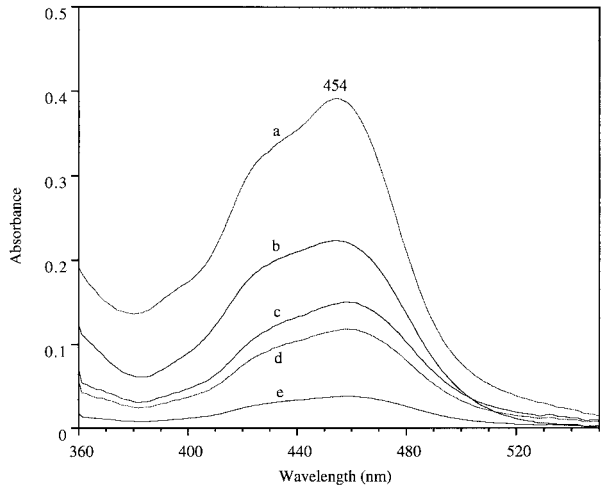

Figure 5. Absorption spectra of polyimide **3**: (a) in degassed MeCN (3×10^{-5} M), (b) on electrode **VI**, (c) on electrode **IV**, (d) electrode **V**, and (e) electrode **III**.

Absorption Spectra of Polymer 3 on Electrodes III−VI. Figure 5 compares the absorption spectrum of polyimide **3** in MeCN and when adsorbed on SnO_2 as in electrodes **III**−**VI**. The absorption maxima at 454 nm and the peak shapes of the MLCT absorption bands from the pendent ruthenium complex when adsorbed on the electrodes are identical with those of polyimide **3** in solution. Thus, no electronic perturbation of polyimide **3** takes place upon adsorption onto SnO_2, either as a single layer in **III** and **IV** or as multiple laminate layers in **V** and **VI**. The absorbance at 454 nm increases linearly with the number of applications of a polymer solution with the same concentration (10 mg/mL), as the absorbances of electrodes **V** (3 layers of polymer, $OD_{454} = 0.117$) and **VI** (4 layers of polymer, $OD_{454} = 0.148$) illustrate. These absorptions are nearly 3 and 4 times that of electrode **III** (1 layer of polymer, $OD_{454} = 0.036$) at this same wavelength.

Fluorescence of 2 and 3 in Solution and on the Electrodes. The fluorescence emission and excitation spectra of polymer **3** in MeCN exhibit the same intensities and maxima as those of **2** at the same chromophore concentration (Figure 6). Although the fluorescence emission spectrum of **3** adsorbed on ITO/SnO_2 (electrode **III**) is identical with that of **2** adsorbed on ITO/SnO_2 (electrode **VII**), the peak maximum (466 nm) in the excitation spectrum of electrode **III** is red-shifted by 12 nm from that of electrode **VII** (Figure 7). Since the peak maximum at 454 nm of **2** on ITO/SnO_2 electrode (**VII**) is identical with that of **2** in MeCN, the pendent ruthenium complexes in **3** must aggregate[27] upon deposition onto the colloidal SnO_2 film.

The fluorescence spectra of electrodes **III**−**VI** are compared with that of **3** on ITO (**VIII**, Figure 8). The characteristic metal-to-ligand charge-transfer (MLCT) state emissions with maxima at 615 nm from derivatized $Ru(bpy)_3^{2+}$ moieties[28] are present in all five electrodes. The intensity variations illustrated in Figure 8 are a consequence of difficulties in quantitative deposition via spin casting of the multilayer films. The shoulder emission at 700 nm present in spectrum of each of the electrodes is absent from the spectrum of **3** in solution (Figure 6a). An analogous red-shoulder has been attributed to an excimer-like emission from stacked aggregates of planar aromatic molecules.[29] Although Kamat et al.[13] did not report an analogous band in the fluorescence spectra of a similar ruthenium(II) complex, bis(2,2′-bipyridine)(2,2′-bipyridine-4,4′-dicarboxylic acid)ruthenium(II) perchlorate ($Ru(bpy)_2(dcby)^{2+}$) on ITO/SnO_2, their spectral measurements did not extend to the wavelengths longer than 700 nm.

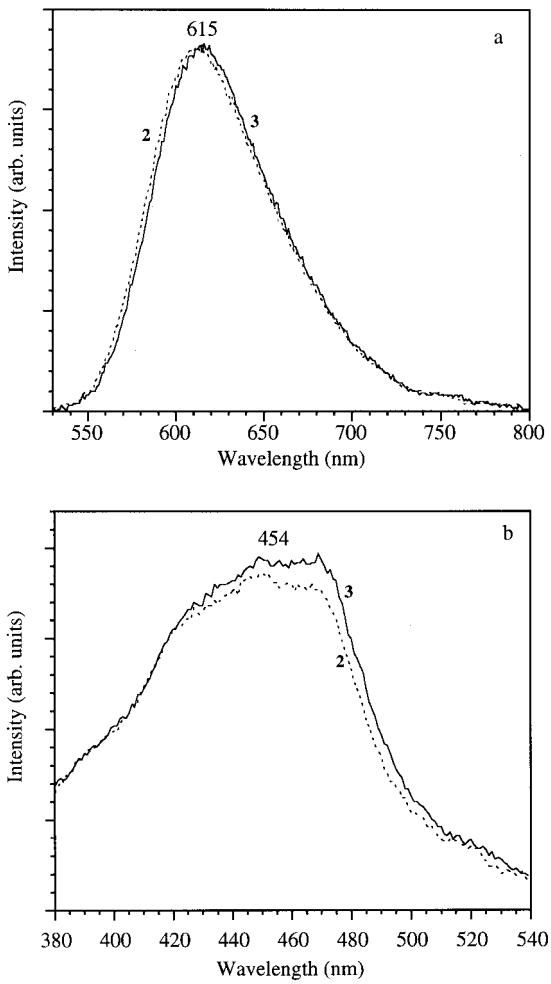

Figure 6. Fluorescence (a) emission ($\lambda_{ex} = 460$ nm) and (b) excitation ($\lambda_{em} = 615$ nm) spectra of **2** (2×10^{-5} M, dash line) and **3** (2×10^{-5} M of $Ru(bpy)_3^{2+}$, solid line) in deoxygenated MeCN at room temperature.

To determine whether the species responsible for the emission at 700 nm differs from that emitting at 615 nm, excitation spectra for electrode **III** were recorded at three different emission wavelengths, 570, 615, and 730 nm (Figure 9). The normalized excitation spectra are very similar with a peak maximum at 466 nm. This observation suggests that the same ground-state species in **3** gives rise to the emissions at both 615 and 730 nm. Identical results were also observed for electrodes **IV**, **V**, and **VI**. The intensity of the shoulder at around 430 nm is slightly higher when the excitation spectrum was monitored at 615 nm than at 570 or 730 nm. (This may be an instrumental artifact because the emitting light is much weaker when monitored at 570 or 730 nm than at 615 nm.)

Cyclic Voltammetry of Complex 2 and of Polyimides 1 and 3. The loading of $Ru(bpy)_3^{2+}$ derivative **2** onto polyimide **1** in polyimide **3** was also confirmed by cyclic voltammetry measurements. Figure 10 shows a cyclic voltammogram of polyimide **3**, the monomeric model compound **2**, and unlabeled polyimide **1**. The peaks between +1.2 and +1.3 V (vs SCE in CH_3CN) are typical of reduction of a substituted Ru(III) complex.[30] Although the observed peak separation (ΔE_p) of 80 ± 2 mV between the anodic and cathodic peaks of **2** is slightly higher than that predicted by the Nernst equation (59 mV) for a completely reversible single-electron process,[30] the

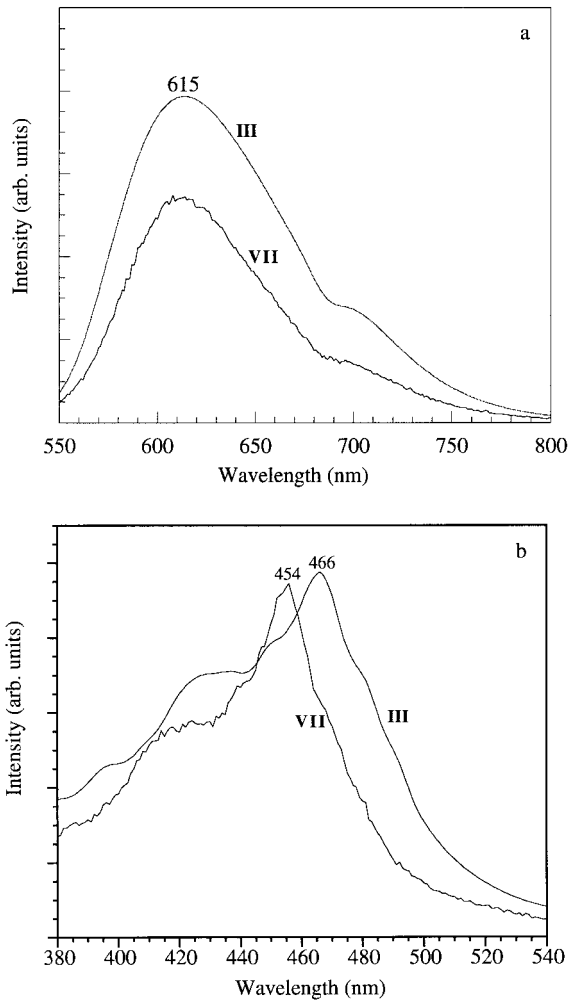

Figure 7. Surface fluorescence (a) emission (λ_{ex} = 460 nm) and (b) excitation (λ_{em} = 615 nm) spectra of **2** on ITO/SnO_2 (electrode **VII**) and **3** on ITO/SnO_2 (electrode **III**) at room temperature.

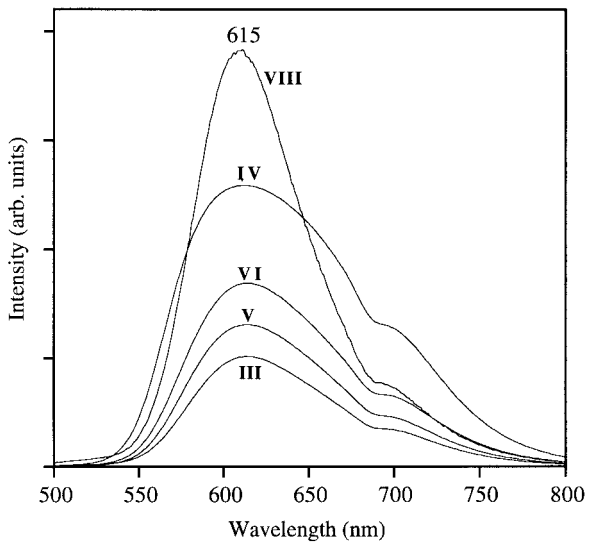

Figure 8. Surface fluorescence emission spectra of polyimide **3** as a thin film on ITO (electrode **VIII**) and on ITO/SnO_2 (electrodes **III**−**VI**).

reductions and oxidations of **2** and **3** are essentially reversible in a polar solvent such as MeCN. The oxidation potential ($E_{1/2}$) of +1.3 V (vs SCE) for polyimide **3** is nearly identical with that of **2** (+1.2 V vs SCE). The close match in the oxidation

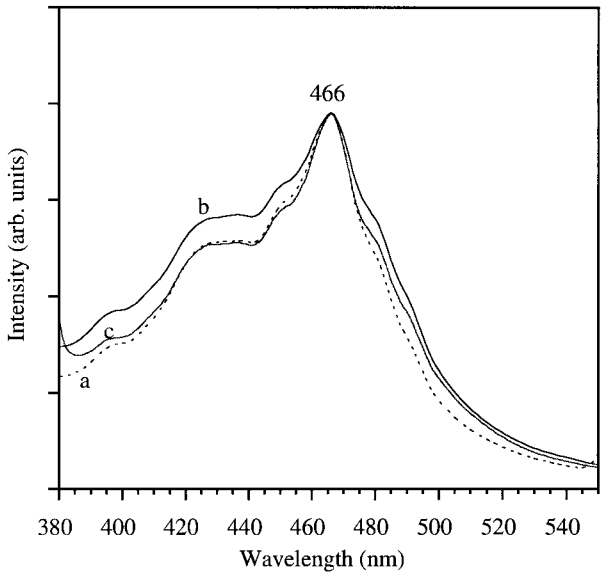

Figure 9. Normalized surface fluorescence excitation spectra (to 466 nm) of electrode **III** at room temperature, λ_{em} = (a) 570, (b) 615, and (c) 730 nm.

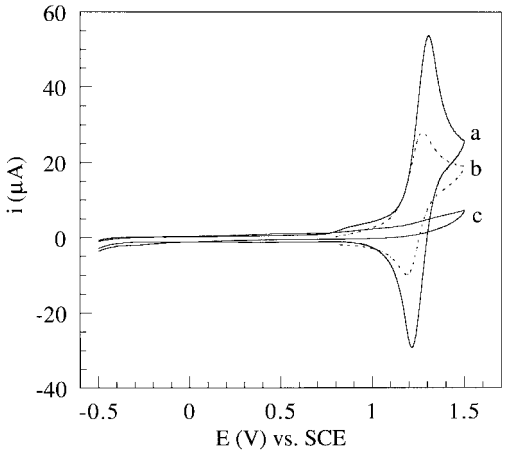

Figure 10. Cyclic voltammetry on a glassy carbon electrode of (a) polyimide **3** (10^{-5} M of $Ru(bpy)_3^{2+}$), (b) complex **2** (5×10^{-3} M), and (c) polyimide **1** in deoxygenated MeCN containing 0.1 M TBAP, with a saturated calomel (SCE) as reference and a Pt wire (about 0.5 cm^2 geometric area) as counter electrode. Scan rate: 50 mV/s.

potential and reversibility of polyimide **3** and complex **2** suggests that the substituted $Ru(bpy)_3^{2+}$ chromophores in polyimide **3** behave electrochemically as distinct redox centers and are unaffected by aggregation in solution in the concentration range and electrolyte used for these electrochemical measurements.[30]

Nearly no redox activity could be observed in the region between −0.5 and +1.5 V (vs SCE) for the parent polyimide **1**. Therefore, there is no direct electrochemical reduction or oxidation of either the substituted $Ru(bpy)_3^{2+}$ groups or the polyimide backbone in the potential range chosen for the photocurrent measurements (−0.4 to +0.3 V (vs Ag/AgCl)).

Photosensitization of Electrode III by Polyimide 3 in a Photoelectrochemical Cell Mechanism for Photocurrent Production. Figure 11[2,3] shows a schematic illustration of the energy levels of a dye-sensitized (S) nanocrystalline SnO_2 film in contact with aqueous H_2Q (0.01 M) containing NaH_2PO_4 (0.05 M), as is found in electrode **III**. The absorption threshold of the attached $Ru(bpy)_3^{2+}$ derivative in **3** adsorbed on ITO/SnO_2 (electrode **III**) is about 550 nm, corresponding to an S^+/S^* transition of +2.3 eV.[3] To this value is added the oxidation

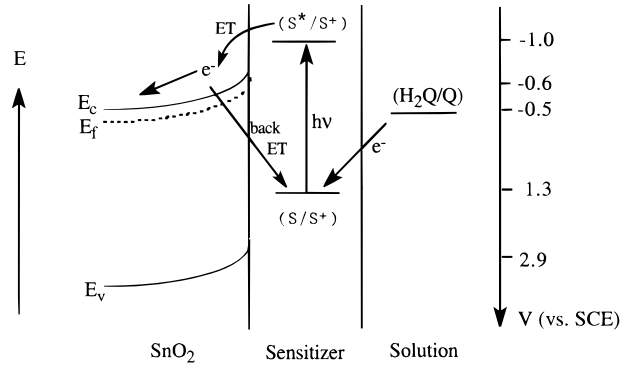

Figure 11. Schematic illustration of photoinduced electron injection in the photosensitization by sensitizer S of a nanocrystalline SnO_2 (n-type) thin-film electrode in contact with an electrolyte (H_2Q). E_c, E_f, and E_v stand for energy levels of the conduction band, the Fermi level, and the valence band of the semiconductor, respectively. S, S^+, and S* stand for sensitizer, oxidized sensitizer, and electronically excited sensitizer, respectively, and e^- represents the mobile electron.[2,3] The half-cell potentials shown at the right indicate ordering of the key half-reactions in relationship to the valence and conduction band edges, all measured in reference to SCE in degassed acetonitrile.

potential of +1.3 V (vs SCE) for the $Ru(bpy)_3^{2+}$ derivative in **3** (Figure 10) to obtain an excited-state reduction potential of −1.0 V (vs SCE) for $Ru(bpy)_3^{3+}/(Ru(bpy)_3^{2+})^*$, slightly negative of the conduction band edge of SnO_2. The bandgap energy for a nanocrystalline semiconductor SnO_2 thin film is about 3.5 eV,[9] with a valence band edge of 2.9 V (vs SCE).[2] The maximum cell voltage expected under illumination with substituted $Ru(bpy)_3^{2+}$-labeled polyimide **3** as photosensitizer corresponds to the difference between the conduction band edge of SnO_2 and the electrochemical potential of the electrolyte, H_2Q (0.01 M) containing NaH_2PO_4 (0.05 M), or 0.12 V for **III** upon irradiation at 460 nm (vide infra).

The lowest energy of electronic transition in $Ru(bpy)_3^{2+}$ derivatives is a metal-to-ligand-charge-transfer (MLCT) state in which one electron is transferred from the excited ruthenium ion to one of the coordinated bipyridyl ligands.[2] Electron injection from this reduced ligand into the conduction band of the SnO_2 nanoparticles then takes place. Back electron transfer to the photooxidized $Ru(bpy)_3^{3+}$ center is suppressed by the presence of H_2Q, which effects a quick reductive regeneration of $Ru(bpy)_3^{2+}$ while being itself oxidized via the semiquinone ultimately to quinone Q. This latter process is responsible for the observation of a steady-state photocurrent across the liquid electrolyte[2] when electrode **III** is irradiated at 460 nm.

Open-Circuit Photovoltage (OCPV) Generation and Short-Circuit Photocurrent (i_{sc}) Characteristics of Electrode III in a Photoelectrochemical Cell. Figure 12 (top) shows a typical open circuit photovoltage response of electrode **III** upon illumination with 460 nm monochromatic light. Photovoltage generation is instantaneous and remains virtually constant over at least several on−off illumination cycles. This observation is consistent with the injection of an electron from the MLCT state of the appended $Ru(bpy)_3^{2+}$ group to the conduction band of the SnO_2 nanoparticle, followed by interparticulate hopping to the conduction band of the ITO-coated glass. After the light is turned off, the photovoltage decays back to zero within seconds.

Characteristic photocurrents observed upon irradiation of electrode **III** under an applied bias of −0.1, 0, and +0.1 V (vs SCE) are shown in Figure 12 (bottom). The observed photocurrents increase as the applied potential of the photoelectrochemical cell is shifted to a more positive bias. Upon

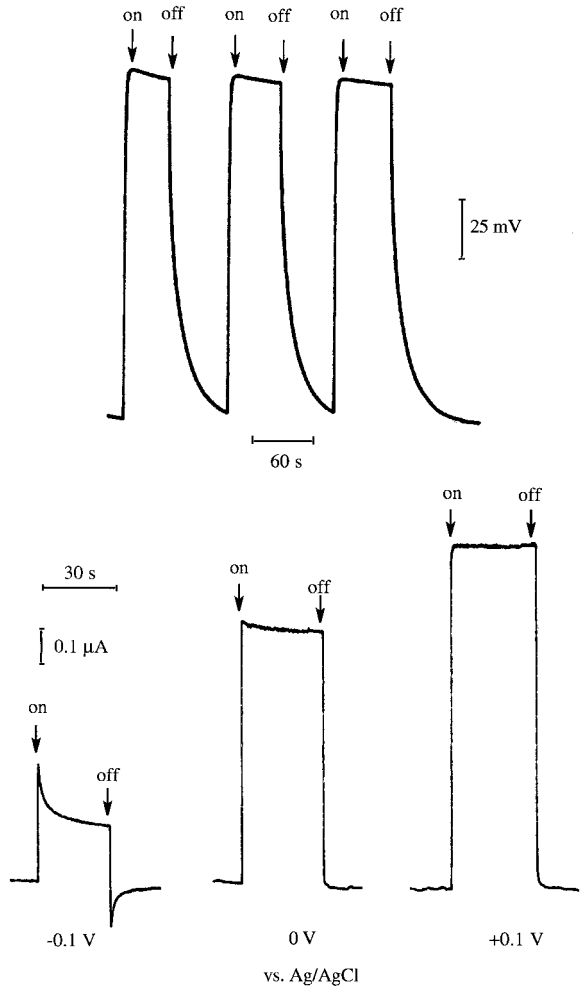

Figure 12. Open-circuit photovoltage (OCPV, top) and sensitized photocurrent (i_{sc}) of a photoelectrochemical cell with electrode **III** as the working electrode measured during several on−off illumination (460 nm, 1.14×10^{-2} mW/cm^2) cycles in deoxygenated aqueous. H_2Q (0.01 M) containing NaH_2PO_4 (0.05 M) at pH of 5.2. The reference and counter electrodes are Ag/AgCl and a Pt wire, respectively.

illumination at 460 nm under a bias of −0.1 V (vs SCE), a decay of anodic photocurrent and a growth of cathodic current upon termination of illumination could be observed. The growth of cathodic current arises from a back electron transfer from reduced SnO_2 nanoparticle to the photooxidized adsorbed dye $Ru(bpy)_3^{3+}$ derivative. The decay of anodic photocurrent under illumination is, however, greatly suppressed at a bias of 0 V (vs SCE) and is completely absent at a bias of +0.1 V (vs SCE), whereas the growth of cathodic current is retarded at a bias of 0 and +0.1 V (vs SCE). This observation clearly indicates that a positive bias facilitates electron transport across the SnO_2 nanoparticulate thin film toward the conducting surface of ITO-coated glass.

Photocurrent Action Spectra and Cell Efficiency. Photocurrent action spectra, i.e., plots of the observed photocurrent as a function of the wavelength of the incident light, of electrodes **III**−**VI** and of relevant electrodes **I** and **II** are shown in Figure 13. No photocurrent was observed upon irradiation at wavelengths longer than 400 nm for either electrode **I** or **II**. The parent polyimide **1** cannot sensitize the ITO/SnO_2 electrode in this wavelength region because it absorbs only at wavelengths shorter than 380 nm (Figure 4), and the onset for direct bandgap excitation of SnO_2 is about 350 nm. On the other hand, the photocurrent action spectra of electrodes **III**−**VI** closely

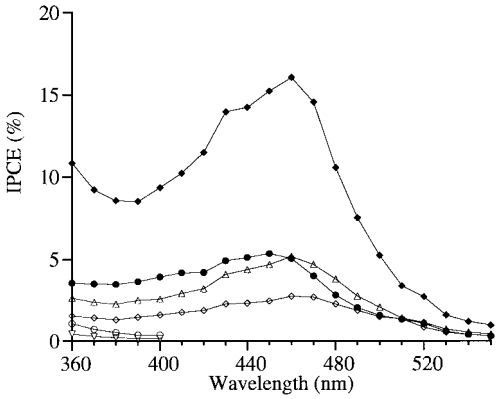

Figure 13. Photocurrent action spectra of electrodes **III** (◆), **IV** (●), **V** (△), **VI** (◇), **I** (○), and **II** (▽). The IPCE values are lower limits as they are not corrected for the loss of light intensity caused by absorption and reflection by the conducting glass support. The size of the working electrode was 0.78 cm^2. The reference and counter electrodes are Ag/AgCl and a Pt wire, respectively. The cell was operated in the short-circuit mode with a bias of 0 V (vs Ag/AgCl).

TABLE 2: Photoelectrochemical Characteristics of Electrodes[a] II−V and Relevant Electrodes[a] I and II upon Illumination at 460 nm[b]

electrode	OCPV (V)[c]	i_{sc} (μA/cm^2)[d]	IPCE (%)[e]
I	0	0	0
II	0	0	0
III	0.12	0.87	16
IV	0.082	0.28	5.1
V	0.10	0.28	5.2
VI	0.076	0.15	2.8

[a] In deoxygenated aqueous H_2Q (0.01 M) in NaH_2PO_4 (0.05 M) at pH of 5.2. [b] Incident light intensity of 1.14×10^{-2} mW/cm^2. [c] Open-circuit photovoltage. [d] Short-circuit photocurrent measured at a bias of 0 V (vs Ag/AgCl). [e] Incident photon-to-current efficiency calculated from eq 1.

resemble the absorption spectra of the polyimide **3** layer, with peak maxima at 454 nm. These action spectra thus indicate successful photosensitization of the electrodes by the pendent $Ru(bpy)_3^{2+}$ chromophores in polyimide **3**.

Photoelectrochemical characteristics, open-circuit photovoltage (OCPV), short-circuit photocurrent (i_{sc}), and IPCE (%) of electrodes **III**−**VI** and their relevant model electrodes **I** and **II** under illumination by monochromatic light at 460 nm are summarized in Table 2. The incident monochromatic photon-to-photocurrent conversion efficiency (IPCE)[2] is defined as the number of electrons produced in the external circuit divided by the number of incident photons, which can be evaluated in eq 1:[13,16]

$$\text{IPCE (\%)} = 100 \times (i_{sc} \times 1240)/(I_{inc} \times \lambda) \qquad (1)$$

where i_{sc} is the short-circuit photocurrent (A/cm^2), I_{inc} is the incident light intensity (W/cm^2), and λ is the excitation wavelength (nm).

Electrode **III** with one polymer layer on a nanoparticular thin layer of SnO_2 has the highest IPCE, whereas the electrodes **IV**, **V**, and **VI**, each with a much higher absorptivity, actually produce lower photocurrents than **III**. For electrodes **V** and **VI** with a laminated structure, the high probability of recombination of the photogenerated electrons and holes as these carriers travel through the laminated polymer and nanoparticulate layers might be responsible for the observed low IPCE values. The low IPCE for electrode **IV** could be explained by the fact that electron injection from excited $Ru(bpy)_3^{2+}$ derivatives takes place only within monolayer coverage on the nanocrystalline particulate thin films, i.e., excited dye molecules beyond monolayer coverage deactivate through pathways other than electron-transfer quenching by the semiconductor nanoparticulate thin films.[31] Photoelectrochemical measurements for modified electrode **VII** could not be carried out because complex **2** quickly desorbs into the aqueous electrolyte.

The maximum IPCE of 16% for monochromatic irradiation of electrode **III** at 460 nm is comparable to the same type of nanocrystalline SnO_2 thin-film electrodes modified with bis(2,2′-bipyridine)(2,2′-bipyridine-4,4′-dicarboxylic acid)ruthenium(II) perchlorate ($Ru(bpy)_2(dcby)^{2+}$) sensitizer in electrolyte I_3^-/I_2 in acetonitrile, in which a maximum IPCE of 22% for monochromatic irradiation at 460 nm was observed.[9] However, the IPCE values for Ru(II) bis(bipyridine) derivatives adsorbed on SnO_2 are lower than those of Ru(II) bis(bipyridine) derivatives adsorbed on TiO_2, in which a monochromatic IPCE of ∼90% at the complex absorption maximum has been reported.[2,8,32]

Conclusions

A substituted $Ru(bpy)_3^{2+}$-labeled polyimide **3** is highly soluble in MeCN, but adsorbs strongly onto a nanocrystalline thin film of SnO_2. The quantitative loading of the ruthenium complex by bonding at the hydroxyl groups of polyimide **1** was confirmed by proton NMR spectra, absorption, and emission spectra, and cyclic voltammetry. Composite SnO_2−**3** thin-film electrodes can be efficiently sensitized when irradiated in the visible. As has been observed with low molecular weight sensitizers adsorbed on nanoporous metal oxide films, the photosensitization takes place by a mechanism involving photoinduced electron injection from the pendent substituted $Ru(bpy)_3^{2+}$ units to the SnO_2 nanoparticles and subsequent electron hopping to the conductive ITO electrode surface. A maximum IPCE of 16% from monochromatic excitation at the absorption maximum of the pendent complex was observed for electrode **III**. Lower efficiencies were observed for the laminate electrodes containing multilayers of **3** and SnO_2. Although no advantage was observed in preparing multilayer composite films **V** and **VI**, these results do demonstrate the viability of polymeric adsorbed photosensitizers for porous nanoparticle metal oxide electrodes.

Acknowledgment. This work was supported by the Texas Advanced Research Program and by the Robert A. Welch Foundation. We are grateful to Professor C. Grant Willson for the use of his DSC and TGA instruments.

References and Notes

(1) Kamat, P. V. *Chem. Rev. (Washington, D.C.)* **1993**, *93*, 267.
(2) Hagfeldt, A.; Grätzel, M. *Chem. Rev. (Washington, D.C.)* **1995**, *95*, 49.
(3) Grätzel, M. *Heterogeneous Photochemical Electron Transfer*; CRC Press: Boca Raton, FL, 1989.
(4) Bard, A. J.; Fox, M. A. *Acc. Chem. Res* **1995**, *28*, 141.
(5) Fox, M. A.; Dulay, M. T. *Chem. Rev. (Washington, D.C.)* **1993**, *93*, 341.
(6) Mills, A.; Davies, R. H.; Worsley, D. *Chem. Soc. Rev.* **1993**, *22*, 417.
(7) Degani, Y.; Willner, I. *J. Am. Chem. Soc.* **1983**, *105*, 6228.
(8) O'Regan, B.; Grätzel, M. *Nature* **1991**, *353*, 737.
(9) Bedja, I.; Hotchandani, S.; Kamat, P. V. *J. Phys. Chem.* **1994**, *98*, 4133.
(10) Vlachopoulos, N.; Liska, P.; Augustynski, J.; Grätzel, M. *J. Am. Chem. Soc.* **1988**, *110*, 1216.
(11) Moser, J.; Grätzel, M. *J. Am. Chem. Soc.* **1984**, *106*, 4336.
(12) Kamat, P. V.; Chauvet, J. P.; Fessenden, R. W. *J. Phys. Chem.* **1986**, *90*, 1398.

(13) Kamat, P. V.; Bedja, I.; Hotchandani, S.; Patterson, L. K. *J. Phys. Chem.* **1996**, *100*, 4900.
(14) Hotchandani, S.; Kamat, P. V. *Chem. Phys. Lett.* **1992**, *191*, 320.
(15) Liu, D.; Kamat, P. V. *J. Electrochem. Soc.* **1995**, *142*, 835.
(16) Nasr, C.; Hotchandani, S.; Kamat, P. V.; Das, S.; Thomas, K. G.; George, M. V. *Langmuir* **1995**, *11*, 1777.
(17) (a) Bedja, I.; Hotchandani, S.; Carpentier, R.; Fessenden, R. W.; Kamat, P. V. *J. Appl. Phys.* **1994**, *75*, 5444. (b) Hotchandani, S.; Das, S.; Thomas, K. G.; George, M. V.; Kamat, P. V. *Res. Chem. Intermed.* **1994**, *20*, 927.
(18) Li, W.; Osoro, H. *J. Photochem. Photobiol. A*, submitted for publication.
(19) Ogawa, S.; Fan, F.-R. F.; Bard, A. J. *J. Phys. Chem.* **1995**, *99*, 11182.
(20) Ho, B.; Lin, Y.; Lee, Y. *J. Appl. Polym. Sci.* **1994**, *53*, 1513.
(21) Sullivan, B. P.; Salmon, D. J.; Meyer, T. J. *Inorg. Chem.* **1978**, *17*, 3334.
(22) Ciana, L. D.; Hamachi, I.; Meyer, T. J. *J. Org. Chem.* **1989**, *54*, 1731.
(23) Younathan, J. N.; McClanahan, S. F.; Meyer, T. J. *Macromolecules* **1989**, *22*, 1048.
(24) Mitsunobu, O. *Synthesis* **1981**, 1.
(25) Kamat, P. V. *CHEMTECH* **1995**, *June*, 22.
(26) Otero, L.; Osora, H.; Li, W.; Fox, M. A. *J. Porph. Phthal.*, in press.
(27) Creed, D.; Griffin, A. C.; Hoyle, C. E.; Venkataram, K. *J. Am. Chem. Soc.* **1990**, *112*, 4049.
(28) Strouse, G. G.; Worl, L. A.; Younathan, J. N.; Meyer, T. J. *J. Am. Chem. Soc.* **1989**, 9101.
(29) Birks, J. B. *Photophysics of Aromatic Molecules*; Wiley: New York, 1970.
(30) Bard, A. J.; Faulkner, L. R. *Electrochemical Methods: Fundamentals and Applications*; Wiley: New York, 1980.
(31) Dabestani, R.; Bard, A. J.; Campion, A.; Fox, M. A.; Mallouk, T. E.; Webber, S. E.; White, J. M. *J. Phys. Chem.* **1988**, *92*, 1872.
(32) Nazeeruddin, M. K.; Kay, A.; Rodicio, I.; Humphry-Baker, R.; Müller, E.; Liska, P.; Vlachopoulos, N.; Gräzel, M. *J. Am. Chem. Soc.* **1993**, *115*, 6382.